(Received 26 May 2024, Accepted 8 July 2024, Scheduled 17 July 2024)

A Dual-Band Four-Port Printed MIMO Antenna with Enhanced Isolation and Polarization Diversity for Midband 5G Applications

Vishnupriya Rajagopalan*, Sanish V. Sanu, and Stephen Rodrigues

Department of Instrumentation, Cochin University of Science and Technology, Cochin, Kerala, India

ABSTRACT: A compact four-port dual-band multiple-input multiple-output (MIMO) antenna system with reduced mutual coupling is proposed in this paper. The dual-band antenna operates in the frequency range covering 3.1–3.6 GHz (5G NR, n78) and in the newly introduced 5G midband spectrum of 5.925–7.125 GHz (5G NR, n96). The proposed MIMO antenna system is compact with dimensions $65 \times 65 \times 0.8\,\text{mm}^3$ and has isolation ≤ -20 dB among all ports. The single monopole antenna is loaded with multiple resonant branches designed and optimized with impedance bandwidths of 14.92% at 3.35 GHz and 18.46% at 6.5 GHz. Impedance bandwidth, polarization diversity, and mutual coupling between elements for the designed four-port MIMO antenna system are measured. The proposed design is fabricated using an FR4 epoxy substrate, and the measured gain values are 3.9 dB and 4.8 dB for 3.3 GHz and 6.5 GHz, respectively, with nearly omnidirectional radiation pattern.

1. INTRODUCTION

The introduction of 5G technology marks the dawn of a new era in connectivity, characterized by high speeds, ultra-low latency, and exceptional network reliability [1]. As data demand grows exponentially, and the number of connected devices proliferates, 5G networks face unprecedented challenges in delivering seamless, high-quality services. The Federal Communications Commission's decision to make 1,200 MHz of spectrum in the 6 GHz band (5.925–7.125 GHz) available for unlicensed use nearly quintuples the spectrum available for Wi-Fi, enhancing connectivity [2]. To meet the demand, high-capacity wireless systems development is desired to accommodate the large number of interconnected devices. Among them, high data rate is the most important requirement, where multiple-input multiple-output (MIMO) systems [3–5] are reported to be a potential technology that employs several diversity techniques [6, 7] to meet the throughput requirements. Nevertheless, MIMO antenna systems are not free from interference, specifically when radiating elements are placed adjacent to each other. Several techniques are adopted to avoid interference and improve performance of such miniaturized systems [8–10].

The diverse radiation pattern of asymmetric radiating elements is utilized to achieve radiation pattern diversity [11]. Recently Zhang et al. proposed a technique to achieve port to port isolation more than 25 dB [12], however at the cost of inclusion of additional probes. Improved mutual coupling reduction can be achieved by the insertion of parasitic strips [13] with additional shorting vias, but it essentially adds complexity to the design.

Employing T-shaped slots and a meandering resonant branch provides high isolation [14]. Isolation can be improved by incorporating multiple ground plane slots and neutralizing lines linking the two symmetric radiating elements [15]; however this approach is limited to two ports. The aforementioned designs discuss several techniques to improve port to port isolation, however, by employing complicated decoupling and matching networks, defected ground structure, electronic band gap structures, modifying ground plane with slots, and parasitic elements. In general, these techniques either add complexity in the design or increase antenna size with bulky structure causing difficulty in fabrication and system integration. This is particularly important while considering the newly introduced spectrum (5.925–7.125 GHz), which is anticipated to enhance connectivity in internet of things (IoT) devices. Although multiband antennas with improved performance have been reported earlier, serving the existing bands and newly introduced spectrum opens new challenges and novel design considerations. Under this backdrop, we present a compact, four-port, dual-band MIMO antenna with polarization diversity and enhanced isolation, suitable for 5G midband spectrum (3.1–3.6 GHz, and 5.925–7.125 GHz) applications. The proposed design is compact and does not employ additional elements despite having exceptional performance characteristics.

2. ANTENNA GEOMETRY AND DESIGN

Printed monopole antennas are a good candidate for MIMO applications. It has several advantages such as compact size, abil-

* Corresponding author: Vishnupriya Rajagopalan (vishnupriya.in@cusat.ac.in).

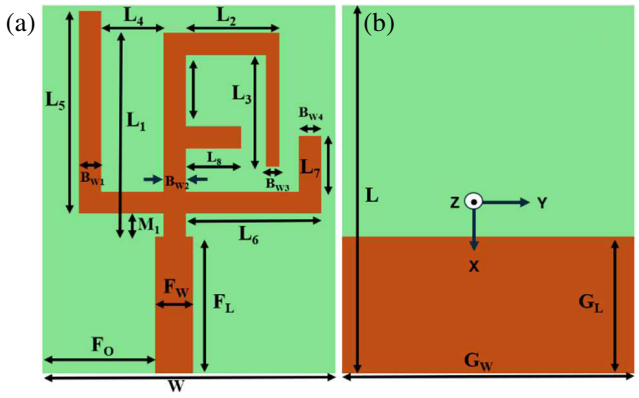

FIGURE 1. Schematic representation of the dual-band monopole antenna. (a) top layer, and (b) bottom layer.

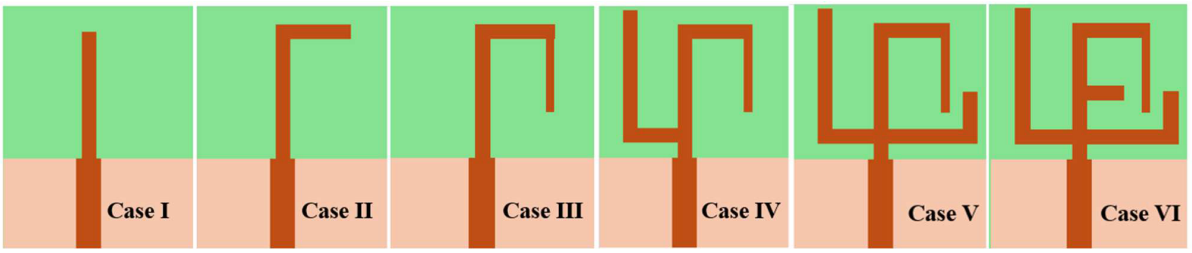

FIGURE 2. Design evolution of the proposed antenna from case I to case VI. The dimensional details are provided in Fig. 1.

ity to generate multiple resonant modes, and wide impedance bandwidth [9].

The present study proposes a dual-band monopole antenna loaded with multiple resonant branches. Fig. 1 shows the geometry of the top and bottom layers of the proposed dual-band monopole antenna suitable for midband 5G application bands, 3.1 to 3.6 GHz, and 5.925 to 7.125 GHz.

The designed antenna is fabricated on a low-cost standard FR4 epoxy substrate with double sided copper cladding (relative permittivity = 4.4, loss tangent = 0.025), which has a total dimension of $33\times24\times0.8$ mm^3. The choice of substrate material for the proposed MIMO antenna system was based on its widespread availability, cost effectiveness compared to other specialized substrates, ease of fabrication for rapid prototyping and small-scale production, good mechanical strength, and thermal stability. The radiator with the microstrip feedline is fabricated on top and the rectangular ground plane on the bottom layers of the dielectric substrate. Copper cladding thickness is 0.035 mm, and its conductivity is 5.96×10^7 S/m. A 50-ohm microstrip transmission line with length F_L and width F_W as shown in Fig. 1 is directly connected to the radiator to excite the suitable resonant modes.

The single monopole antenna is realized from multiple metal strips or resonant branches with different lengths. Since each branch acts as a resonating element, the length, width, and position of each resonating element needs to be optimized to achieve the required impedance bandwidth. It is important to note that the length of the resonant branches are multiples of $\lambda_g/4$, where λ_g is the guided wavelength for the corresponding resonant frequency.

The antenna design evolution is illustrated in Fig. 2. The design started with the construction of a quarter wavelength monopole antenna with length L_1 directly connected to a 50-ohm matched microstrip feedline (case I). For full-wave 3D electromagnetic analysis, simulations employing finite integration technique (FIT) were performed in CST Microwave Studio, to show that the proposed monopole antenna has its first resonance at 3.3 GHz frequency. To create the second band of the midband 5G frequency ranging from 5.925 to 7.125 GHz requires additional resonant modes to be added to the basic quarter wavelength monopole antenna. Such resonant modes can be generated by adding additional surface current paths with different directions and dimensions. The basic quarter wavelength monopole is converted into an inverted L antenna whose resonant frequency is controlled by branches of lengths L_1 and L_2 (case II).

The inverted L antenna shown in case II generates the dual bands. Further, for frequency tuning, an additional branch element with length L_3 is placed at the open end of the horizontal arm of the inverted L antenna. By placing this third branch vertically down, the requirement of extra space that would have been needed while extending horizontal arm is eliminated (case III). L_2 and L_3 together provide the required surface current path which leads to the formation of a new resonant mode at 6.4 GHz. It is important to note that, here, $L_2+ L_3 \approx 3\lambda_g/4$, where λ_g is the guided wavelength at 6.4 GHz.

A separate L-shaped branch with dimensions L_4 and L_5 (case IV), at the bottom left of the quarter wavelength monopole creates an additional L-shaped current path. The lengths L_4 and L_5 are optimized for the excitation of a quarter wavelength res-

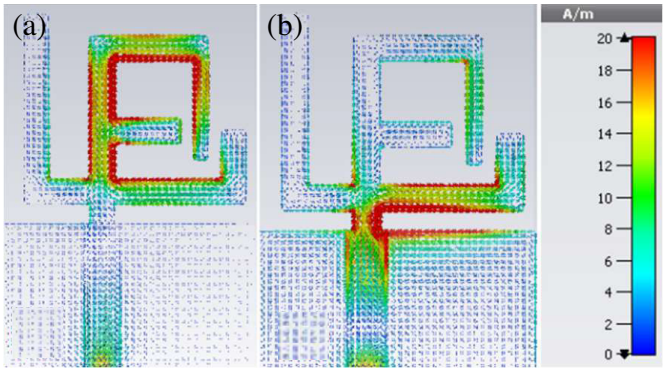

FIGURE 3. Surface current distribution on different branches of monopole antenna for the design case VI of Fig. 2, at (a) 3.3 GHz and (b) 6.8 GHz.

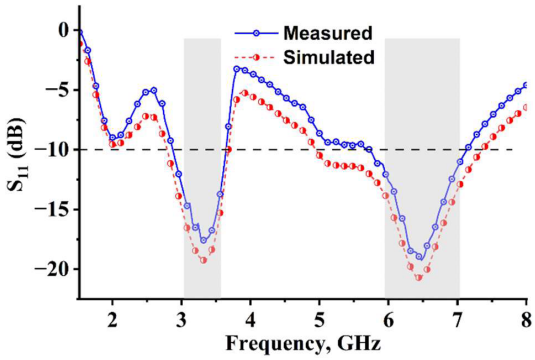

FIGURE 4. Simulated and measured reflection coefficient (S_{11}) of the monopole antenna.

onant mode at 6 GHz. Here, $L_4 + L_5 \approx 3\lambda_g/4$, where λg is the guided wavelength at 6 GHz.

To attain sufficient bandwidth for the second band, an additional L-shaped branch with dimensions L_6 and L_7 is inserted at the bottom right of the basic monopole antenna (case V). The dimensions of L_6 and L_7 are optimized to achieve the required resonance centered at 6.8 GHz. This additional L-shaped current path supports the excitation of another odd resonant mode with $L_6 + L_7 \approx 3\lambda_g/4$, where λ_g is the guided wavelength at 6.8 GHz. The presence of these additional L branches does not have any effect on the lower 3.3 GHz band. In addition, it supports bandwidth enhancement through merging all the three resonant modes at 6 GHz, 6.4 GHz, and 6.8 GHz and thereby generating a wide bandwidth from 5.925 to 7.125 GHz, essential for midband 5G applications. To enhance the smooth transition of the resonance at 5.7 GHz, an additional quarter wavelength element with length L_8, as shown in case VI, is added to the basic monopole antenna. Since the ground plane has a significant role in controlling the impedance bandwidth, its length G_L, width G_W, and feed-offset F_O, as shown in Fig. 1(a), are optimized accordingly. The optimized dimensions of the antenna geometry are given in Table 1.

TABLE 1. Dimensions of the proposed antenna.

Parameter	Dimension (mm)	Parameter	Dimension (mm)
L	33	L_2	8.5
W	24	L_3	9
F_L	13	L_4	3.8
F_W	3	L_5	17
F_O	8.5	L_6	12.2
G_L	13	L_7	4.5
G_W	24	L_8	6.2
L_1	17.2	BW_1	2
BW_2	2	BW_3	1
BW_4	2	M_1	2

To better understand the working mechanism of the proposed planar monopole antenna, the simulated surface current distributions in CST Microwave Studio for two different operation frequencies are studied.

Figure 3 shows the dispersion of surface current from the microstrip line feed to the radiating elements at different frequencies. The study of surface current distribution is crucial, because it is responsible for radiation and reception. The distribution and intensity of these currents at different monopole branches determine the far-field radiation pattern. In Fig. 3(a), the flow of surface current through the quarter wavelength monopole and connected branches is depicted. The longer current path leads to a low frequency resonance at 3.3 GHz. Fig. 3(b) shows that a considerable amount of surface current flows through the horizontal L-shaped branch, resulting in resonance at 6.8 GHz, while the current flow along other branches is negligible. Proceeding with further analysis, the simulated and measured return loss characteristics of the isolated monopole antenna are shown in Fig. 4. It has two resonant bands with the resonant frequency of the first band centered at 3.35 GHz (Impedance Bandwidth = 14.92%) and the resonant frequency of the second band centered at 6.5 GHz (Impedance Bandwidth = 18.46%). Simulated results are in good agreement with the measured ones.

3. INTEGRATION OF FOUR ELEMENT ANTENNA

The antenna element discussed in Section 2 is suitable for midband 5G applications, and to realize the proposed MIMO antenna system, four monopole antennas are arranged in a particular manner as shown in Fig. 5. The four element MIMO antenna is printed on the top layer of a partially grounded FR4 epoxy substrate with dimensions $65\times65\times0.8$ mm^3. In a practical MIMO antenna system, the reduction of mutual coupling between closely placed radiators and improved inter element isolation is crucial especially for applications where space is a constraint. Signal correlation between adjacent antenna elements placed in a compact electrical area leads to unwanted

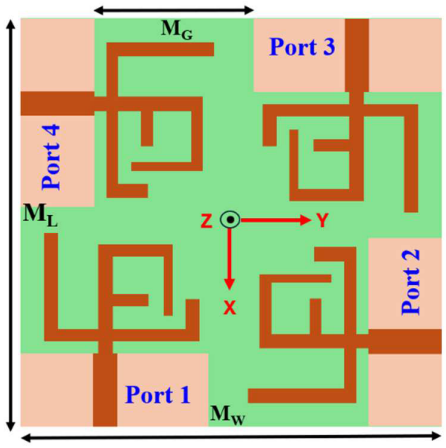

FIGURE 5. The geometry of the proposed MIMO antenna with ports 1–4. The antenna 1–4 are arranged counterclockwise from left bottom of the structure. $M_L = M_W = 65$ mm, $M_G = 28$ mm.

inter-element coupling that degrades MIMO antenna performance.

The overall performance of a MIMO antenna system depends on various factors such as port to port isolation, envelope correlation, impedance bandwidth, radiation efficiency, and diversity techniques. Inclusion of additional ground plane slits and metal strips in between the elements are avoided in the presented design because it may couple fed and act as a resonator leading to a shift in the resonant frequency and alter the impedance bandwidth even if mutual coupling is suppressed. An important parameter causing the inter-element coupling is the common ground that shares the ground plane surface current. This can be avoided by creating individual isolated ground planes for separate elements. The proposed ground plane with optimized dimensions is shown in Fig. 1(b).

To improve the isolation between ports, two different techniques have been used. The first technique is to use separate ground planes instead of a common ground plane so that their ground plane surface currents will not be shared. Fig. 5 shows the separated ground plane geometry. Each adjacent ground plane is separated with a distance of $M_G = 28$ mm to avoid surface current sharing. The second technique is by arranging adjacent elements in perpendicular positions to achieve dual polarizations. Antenna elements arranged with sufficient distance between them help in reducing mutual coupling. Signal correlation between adjacent elements is controlled by its inter-element spacing, and an increase in this will provide low signal correlation, but at the cost of overall size of the MIMO antenna. The optimized value for the spacing is set as $0.1\lambda_0$, where λ_0 is the free space wavelength of the lowest operating frequency.

Arraying elements in orthogonal positions provide lower mutual coupling than those arrayed in parallel positions, in addition to the orthogonal polarization of radiated signals. Antenna 1 is fed from the positive X axis as shown in Fig. 5. The E field polarizations of this antenna are aligned with the X axis, and it radiates upward (positive Z direction), then the E field plane is the XZ plane. Since E and H are orthogonal, the H field is oriented along the Y axis, and H plane is the YZ plane. In this case, antenna 1 is vertically polarized. Antenna 2 is fed from positive Y axis, and E field polarizations of this antenna are aligned with the Y axis. It radiates upward, then the E field plane is the YZ plane, and the H field plane is the XZ plane. In this case, antenna 2 is horizontally polarized. Antenna 3 is vertically polarized, and antenna 4 is horizontally polarized. They are identically fed, similar to antennas 1 & 2, respectively. Polarization diversity is achieved in this way. Hence, antennas 1 and 2 have orthogonal polarization planes, which ensures least coupling. Similar polarization diversity can be achieved between antennas 3 and 4. Thus, both the near field and far field couplings are well suppressed by applying space diversity, polarization diversity, and separated ground planes.

4. RESULTS AND DISCUSSIONS

4.1. IMPEDANCE PERFORMANCE

To evaluate the reflection coefficient (S_{11}) characteristics of the MIMO antenna system, port 1 associated with antenna 1 is excited, and all other ports are matched terminated with 50-ohm impedance. To validate the simulation results, we have used Rohde and Schwarz, ZNB-40 vector network analyzer and measured the S parameters. The same procedure is followed for ports 2, 3, and 4. It is observed that $S_{11} = S_{22} = S_{33} = S_{44}$. Fig. 4 shows the simulated and measured return loss characteristics of antenna 1 corresponding to the excitation of port 1. It can be further observed from Fig. 4 that the operating frequency range of the MIMO system is 3.1–3.6 GHz with an impedance bandwidth of 14.92% and 5.925–7.125 GHz with an impedance bandwidth of 18.46%. Measured results match well with the simulated ones, and these frequency bands cover the 5G mid-band spectrum.

4.2. ISOLATION PERFORMANCE

Figures 6 and 7 show the simulated and measured isolations between different ports. Throughout the operating band mutual coupling between all antenna pairs (1–2, 1–3, 1–4, 2–3, 2–4, 3–4) is ≤ -20 dB without adding any decoupling structures. Also, at the second band, the mutual coupling between all ports decreases further, and the minimum isolation obtained is -23 dB. Since the coupling current is weak, inter-element isolation performance is better for both the bands.

This is achieved by employing separated ground planes, placing elements in perpendicular positions and keeping adequate distance between the elements. It may be noted that the maximum isolation obtained is between the diagonally placed antenna pairs 1–3 and 2–4, i.e., $S_{13} = S_{24} \leq -37$ dB at 7.125 GHz.

The comparison of Figs. 6 and 7 shows that the simulated inter-element isolation levels match the measured results. Only mutual coupling levels of ports 2, 3, and 4 with respect to port 1 are shown. The remaining port combinations also have similar isolation performance. Since all antenna elements are placed in a separated ground environment, the surface current flowing in one ground plane does not affect other elements, which would have degraded isolation and radiation characteristics. Through a systematic design procedure, all the ground planes and ra-

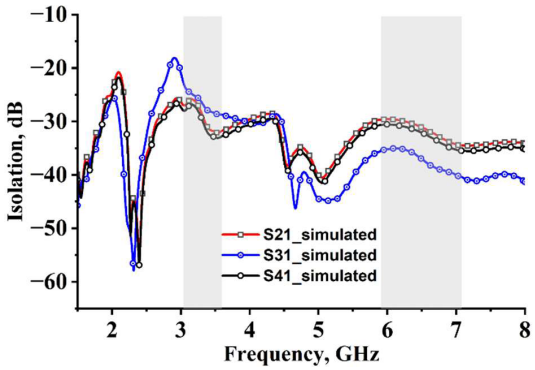

FIGURE 6. Simulated isolation between different ports.

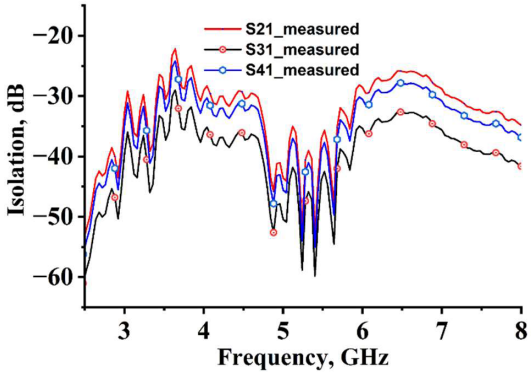

FIGURE 7. Measured isolation between different ports.

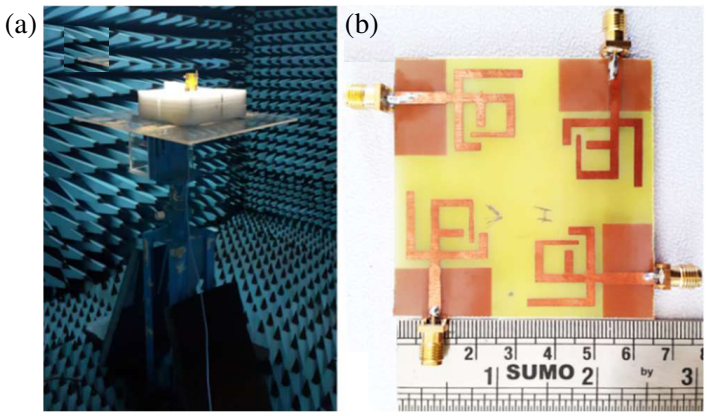

FIGURE 8. (a) Prototype inside the anechoic chamber during measurement (b) fabricated MIMO antenna.

diating elements are included in a compact electrical area of 65×65 mm^2.

4.3. RADIATION PERFORMANCE

Radiation characteristics for the proposed MIMO antenna along XZ plane and YZ plane are performed inside an anechoic chamber. Fig. 8 shows the fabricated prototype of the MIMO antenna system inside the anechoic chamber with port 1 excited and all other ports terminated with matched 50-ohm impedance.

It is important to notice the orientation of the MIMO antenna with respect to the XYZ Cartesian coordinates shown in Fig. 5. The normalized gain radiation patterns for E plane and H plane at 3.3 and 6.5 GHz for port 1 and port 2 are shown in Fig. 9. E plane and H plane radiation patterns of antennas 1 and 3 (vertically polarized) are identical, and antennas 2 and 4 (horizontally polarized) are identical. Since they are diagonal elements, spacing between them is high compared to the adjacent antenna. Edge to edge separation is $0.26\lambda_0$. So, for these element pairs, isolation is achieved by space diversity. Also, E plane and H plane radiation patterns of antennas 1 and 3 are the reverse of antennas 2 and 4. Such combinations with diverse radiation patterns can avoid far-field coupling. In the far field, the planes where element 1's electric field is dominant coincide with that of element 2's electric field that is non-dominant. It results in very negligible signal correlation. The same is valid for element pairs 2–3, 3–4, and 1–4.

Radiation patterns of elements 3 and 4 are not shown as they are the same as elements 1 and 2, respectively, and it has stable gain throughout the midband 5G spectrum. Both E plane and H plane radiation patterns vary within ±1 dB throughout 3.3 GHz lower band, and ±1.4 dB throughout 6.5 GHz higher band. The measured peak gain is 3.9 dB and 4.8 dB for 3.3 GHz and 6.5 GHz, respectively, with nearly omnidirectional radiation pattern. The average radiation efficiency is 74% for the lower band and 59% for the higher band. The reduction in efficiency at the higher frequencies is due to the increased dielectric loss.

4.4. DIVERSITY PERFORMANCE

In scattering environments, such as in mobile communications and deployment of IoT devices, the signal correlation between antennas is highly important, usually estimated using the S-parameters. Often the loss correlation of the antenna is neglected while considering the high radiation efficiency [16]. We estimate the envelope correlation coefficient (ECC) using [17].

$$ECC = \frac{|S_{11}^{*}S_{12}+S_{21}^{*}S_{22}|^2}{(1-|S_{11}|^2-|S_{21}|^2)(1-|S_{11}|^2-|S_{12}|^2)} \quad (1)$$

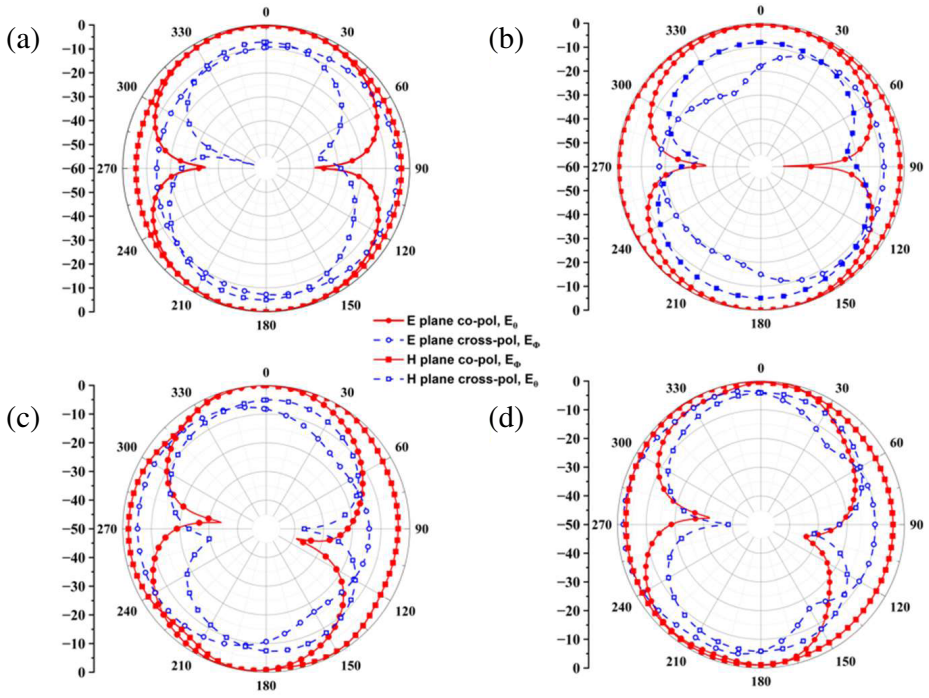

FIGURE 9. Measured E Plane and H Plane radiation patterns at XZ Plane and YZ Plane for (a) Port 1 at 3.3 GHz (b) port 2 at 3.3 GHz (c) port 1 at 6.5 GHz, and (d) port 2 at 6.5 GHz.

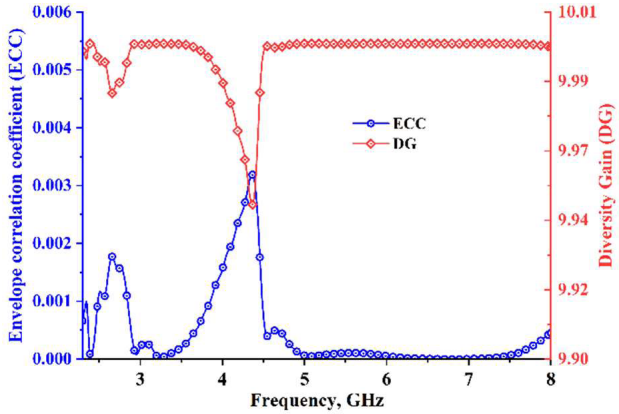

FIGURE 10. Estimated envelope correlation coefficient and diversity gain.

TABLE 2. Comparison of the proposed design with previously reported designs.

Ref.	Antenna size (mm^2)	Frequency (GHz)	Isolation (dB)	ECC
[14]	77.5×52	2.4–2.48	≈ 15	< 0.2
		5.15–5.82		
[18]	40×32	5.1–5.9	> 50	< 0.15
[19]	136×68	3.55–4.2	> 10	< 0.1
		3.6–4.2		
		4.4–4.9		
		5.15–5.925		
[20]	75×37.5	3.3–5.95	> 15	< 0.11
This work	65×65	3.1–3.6	> 22	0.006
		5.9–7.1		

Figure 10 shows that the ECC is well below 0.005. Although several structures of variations are visible, the proposed design provides exceptionally low ECC at the desired band, indicating that the individual elements are uncorrelated with measured isolation less than 20 dB, in highly scattering environments, a crucial requirement for very dense 5G applications. The diversity gain (DG) of the antenna is estimated from ECC following Eq. (2) of [18] and is plotted in Fig. 10. The DG is above ≈ 9.9 for the two operating bands. A comparison of the proposed design with previously reported designs is given in Table 2.

5. CONCLUSION

A dual-band (3.1–3.6 GHz and 5.925–7.125 GHz) four-port MIMO planar monopole antenna suitable for midband 5G applications is presented. The four-element MIMO antenna is realized by arranging monopole antennas in orthogonal positions with a separated ground plane for individual antennas to avoid signal correlation. This ensures a minimum isolation of ≤ -20 dB and ECC lower than 0.005 for the designed band. Measured results show that the MIMO system has an impedance bandwidth of 14.92% at 3.35 GHz, 18.46% at 6.5 GHz and provides a gain of 3.9 dB and 4.8 dB for 3.3 GHz and 6.5 GHz, respectively, with nearly omnidirectional radiation pattern. These performances are achieved even at low element spacing of $0.1\lambda_0$. One promising area for future research is the scalability of the antenna design with eight elements for different applications. This involves optimizing the design for various scales which covers compact devices and IoT gadgets.

REFERENCES

[1] Dahlman, E., S. Parkvall, and J. Skold, *5G NR: The Next Generation Wireless Access Technology*, Academic Press, 2020.

[2] Federal Communications Commission, "FCC opens 6 GHz band to Wi-Fi and other unlicensed uses," Available: https://docs.fcc.gov/public/attachments/DOC-363945A1.pdf.

[3] Hong, W., Z. H. Jiang, C. Yu, J. Zhou, P. Chen, Z. Yu, H. Zhang, B. Yang, X. Pang, M. Jiang, and a. et "Multibeam antenna technologies for 5G wireless communications," *IEEE Transactions on Antennas and Propagation*, Vol. 65, No. 12, 6231–6249, 2017.

[4] Ghosh, A., A. Maeder, M. Baker, and D. Chandramouli, "5G evolution: A view on 5G cellular technology beyond 3GPP release 15," *IEEE Access*, Vol. 7, 127 639–127 651, 2019.

[5] Vook, F. W., A. Ghosh, and T. A. Thomas, "MIMO and beamforming solutions for 5G technology," in *2014 IEEE MTT-S International Microwave Symposium (IMS2014)*, 1–4, Tampa, FL, USA, 2014.

[6] Saurav, K., N. K. Mallat, and Y. M. M. Antar, "A three-port polarization and pattern diversity ring antenna," *IEEE Antennas and Wireless Propagation Letters*, Vol. 17, No. 7, 1324–1328, 2018.

[7] Sharma, Y., D. Sarkar, K. Saurav, and K. V. Srivastava, "Three-element MIMO antenna system with pattern and polarization diversity for WLAN applications," *IEEE Antennas and Wireless Propagation Letters*, Vol. 16, 1163–1166, 2016.

[8] Malik, J., A. Patnaik, and M. V. Kartikeyan, "Novel printed MIMO antenna with pattern and polarization diversity," *IEEE Antennas and Wireless Propagation Letters*, Vol. 14, 739–742, 2014.

[9] Sarkar, D. and K. V. Srivastava, "A compact four-element MIMO/diversity antenna with enhanced bandwidth," *IEEE Antennas and Wireless Propagation Letters*, Vol. 16, 2469–2472, 2017.

[10] Soltani, S., P. Lotfi, and R. D. Murch, "A dual-band multiport MIMO slot antenna for WLAN applications," *IEEE Antennas and Wireless Propagation Letters*, Vol. 16, 529–532, 2016.

[11] Anitha, R., P. V. Vinesh, S. Mathew, P. Mohanan, and K. Vasudevan, "Collocated MIMO antenna with reduced mutual coupling using square ring DGS," *Progress In Electromagnetics Research C*, Vol. 53, 119–125, 2014.

[12] Zhang, W., J. Hu, Y. Li, and Z. Zhang, "Design of a stacked co-polarized full-duplex antenna with broadside radiation," *IEEE Transactions on Antennas and Propagation*, Vol. 69, No. 11, 7111–7118, 2021.

[13] Wei, K. and B.-C. Zhu, "The novel W parasitic strip for the circularly polarized microstrip antennas design and the mutual coupling reduction between them," *IEEE Transactions on Antennas and Propagation*, Vol. 67, No. 2, 804–813, 2019.

[14] Deng, J., J. Li, L. Zhao, and L. Guo, "A dual-band inverted-F MIMO antenna with enhanced isolation for WLAN applications," *IEEE Antennas and Wireless Propagation Letters*, Vol. 16, 2270–2273, 2017.

[15] Yang, Y., Q. Chu, and C. Mao, "Multiband MIMO antenna for GSM, DCS, and LTE indoor applications," *IEEE Antennas and Wireless Propagation Letters*, Vol. 15, 1573–1576, 2016.

[16] Choukiker, Y. K., S. K. Sharma, and S. K. Behera, "Hybrid fractal shape planar monopole antenna covering multiband wireless communications with MIMO implementation for handheld mobile devices," *IEEE Transactions on Antennas and Propagation*, Vol. 62, No. 3, 1483–1488, 2014.

[17] Hallbjorner, P., "The significance of radiation efficiencies when using S-parameters to calculate the received signal correlation from two antennas," *IEEE Antennas and Wireless Propagation Letters*, Vol. 4, 97–99, 2005.

[18] Ghannad, A. A., M. Khalily, P. Xiao, R. Tafazolli, and A. A. Kishk, "Enhanced matching and vialess decoupling of nearby patch antennas for MIMO system," *IEEE Antennas and Wireless Propagation Letters*, Vol. 18, No. 6, 1066–1070, 2019.

[19] Liu, H.-Y., C.-Y.-D. Sim, and C.-J. Huang, "Wideband MIMO antenna array design for future mobile devices operating in the 5G NR frequency bands n77/n78/n79 and LTE band 46," *IEEE Antennas and Wireless Propagation Letters*, Vol. 19, No. 1, 74–78, 2020.

[20] Hei, Y. Q., J. G. He, and W. T. Li, "Wideband decoupled 8-element MIMO antenna for 5G mobile terminal applications," *IEEE Antennas and Wireless Propagation Letters*, Vol. 20, No. 8, 1448–1452, 2021.